SAGE Publishing

Research Article
Adsorption Performance of La(III) and Y(III) on Orange Peel: Impact of Experimental Variables, Isotherms, and Kinetics

Li Liu [ID]**, Yunzhang Rao, Changshun Tian** [ID]**, Tao Huang, Jiacheng Lu, Meidao Zhang, and Min Han**

School of Resources and Environment Engineering, Jiangxi University of Science and Technology, Ganzhou 341000, China

Correspondence should be addressed to Changshun Tian; 9320090329@jxust.edu.cn

To alleviate the environmental problem associated with rare earth wastewater, this research applied waste orange peel (OP) for the adsorption of La(III) and Y(III) from aqueous solution. The adsorption properties of orange peel are characterized using scanning electron microscopy (SEM) and Fourier transform infrared spectroscopy (FTIR), and the participation of hydroxyl and other oxygen-containing groups that promote the physical-chemical interaction is verified. Batch adsorption results suggest that orange peel possesses a satisfactory adsorption performance for La(III) and Y(III). The optimal adsorption conditions were obtained at pH of 6, temperature of 40°C, appropriate dosage of 2 g/L and 3 g/L, contact time of 30 min, and initial ion concentration of 32 mg/L. Under the same condition, adsorption performance of La(III) is better than that of Y(III). The experimental data is well fitted by the Langmuir isotherm model with correlation coefficient $(R^2) > 0.9$ and the minimum standard error values. Equilibrium results show that Langmuir monolayer adsorption capacity of La(III) and Y(III) onto orange peel is up to 37.61 and 31.10 mg/g. The fitting results of kinetics prove that the adsorption process of La(III) and Y(III) follows the pseudosecond-order model. Thus, natural orange peel as a recyclable biosorbent has potential economic and applicative benefits to remove La(III) and Y(III) from aqueous solutions.

1. Introduction

Ion-adsorbed earth ore is one of the most crucial mineral resources in the world. It is increasingly frequent to generate massive volumes of rare earth wastewater on account of continuous mining and smelting [1, 2]. Contaminated water from a mine in southern Jiangxi was measured that contained various rare earth elements (REEs), especially the higher concentrations of lanthanum and yttrium [3]. Slightly toxic REEs will accumulate once into living organisms and cannot be metabolized coupled with chronic ingestion, leading to the detrimental ecosystems and human health [4, 5].

The biosorption method is widely applied in the beneficiation and recovery of REEs [6, 7] by virtue of its advantages such as low cost, easy availability, high efficiency, and ecofriendliness [8]. For the porous surface and abundant adsorption functional groups with strong binding ability containing a carboxyl group, hydroxyl group, and amide

group [9], orange peel (OP) is an exemplary candidate to deploy the adsorption technology for the mitigation of wastewater pollution; their biosorption studies have been mainly focused on heavy metals [10], organic drug [11], toxic oxyanions [12], and dyeing [13] wastewater. Nevertheless, there are a few reports concerning rare earth wastewater remediation [14, 15]. The majority of studies have focused on modifying with OP to improve the adsorption capacity, and the modification methods mainly include acid [16], alkali [17], salt [18], structure [19], carbonization [20], organic solvents [21], and compound modification [22]. The whole preparation process of modified OP is shown in Figure 1. In the complex operating process, large numbers of chemical reagents and distilled water are consumed for repeated immersion and washing. Furthermore, the biological structure of OP is easily destroyed [23], which is challenging to ensure the stability of adsorption performance and reuse. Thereby, the disadvantages of time consuming
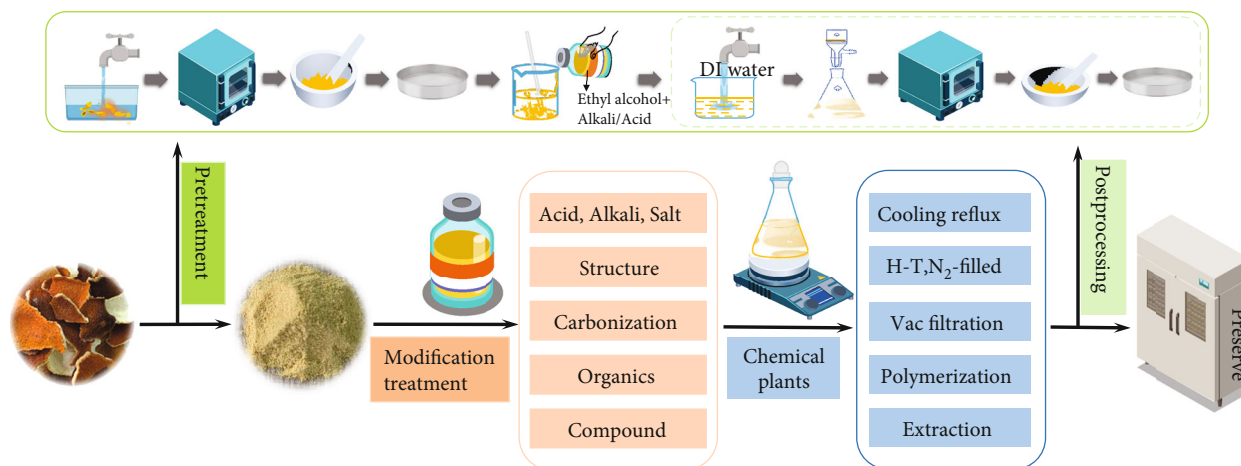
Figure 1: Preparation steps of modified OP.

and low yield indicate that the modification method is not advisable under certain conditions. Feng et al. [24, 25] obtained final modified OP products after undergoing multistep operation with much ethanol, NaOH, and other modifiers to soak for more than 20 h. Zhang et al. [26] studied the effects of activators by preparing activated carbon from citrus peel residue, and the yield was only about 37%. Similarly, Xie et al. [27] applied OP to prepare activated carbon with the highest yield of 50.9%. In addition, when it comes to organic modification, given the deficiency of biodegradability for some typical organic solvents like thioglycolic acid, formaldehyde acrylamide, and others, which brings about hazard of toxic substances and the whole process costs elevated.

In view of this, the adsorption properties of La(III) and Y(III) ions onto unmodified OP from aqueous solutions are investigated with characterization methods and varying conditions. This study is aimed at moderating rare earth wastewater pollution and addressing agricultural waste disposal, so as to provide theoretical and practical guidance for the application of OP in rare earth wastewater treatment.

2. Materials and Methods

2.1. Adsorbent Preparation. Orange peel was collected from an orchard in Ganzhou City, China. The peels were rinsed repeatedly without removing white pith, after which they were air dried and later oven dried at 65°C for constant weight. The dried peels were further ground into fine powder and sieved with particle size in the range of 125 to 150 μm. This powder was stored in PVC plastic bag for standby application. All chemicals used were of analytical grade. The pH was adjusted by adding either NaOH or HCl. Rare earth stock solutions of 5 g/L were prepared with lanthanum(III) sulfate octahydrate (99.99% La) and yttrium(III) sulfate octahydrate (99.99% Y) and diluted to desired concentration.

2.2. Characterization of the Prepared Adsorbent. A scanning electron microscope (SEM) (XL30 W/TMP, Philips, Netherlands) is used to assess the changes of the OP surface mor-

phology before and after adsorption. The spectra of the adsorbents are recorded by the Nicolet Fourier infrared spectrometer (FTIR) in the wavelength range of 400-4000 cm^{-1}, which can identify the affinity between the various functional groups of OP and that adsorption process for La(III) and Y(III).

2.3. Batch Adsorption Experiments. Adsorption experiments were performed in a set of 250 mL stoppered conical flasks by adding 0.15 g OP to 100 mL rare earth solutions with initial concentration of 32 mg/L at pH 6, and then, the solution was stirred for 120 min in constant speed agitators at room temperature. Selectivity adsorption experiments at different parameters were carried out to establish the optimal adsorption conditions. The effects of different experimental conditions on adsorption of OP were investigated by varying initial pH from 2 to 7, dosage of OP from 0.05 g to 0.5 g/100 mL, and repeating experiment between 20 and 50°C. The various initial concentration of rare earth ions ranged from 5 to 100 mg/L for isothermal adsorption study, and the kinetic study was carried out by varying contact time between 2.5 and 120 min. After reaching the preset contact time, a small number of supernatant solutions were filtered immediately.

The residual concentration of rare earth ions after adsorption is detected by spectrophotometer (UV-5100). The adsorption capacity (q_e, mg/g) and adsorption rate (η, %) are calculated by the following equations:

$$q_e = \frac{(C_0 - C_e)V}{M},\qquad(1)$$

$$\eta = \left[\frac{C_0 - C_e}{C_0}\right]\cdot100,\qquad(2)$$

where C_0 and C_e (mg/L) are the initial and final or equilibrium REE concentration in solution, respectively; V (L) denotes the volume of solution; and M (g) refers to the mass of OP powder.
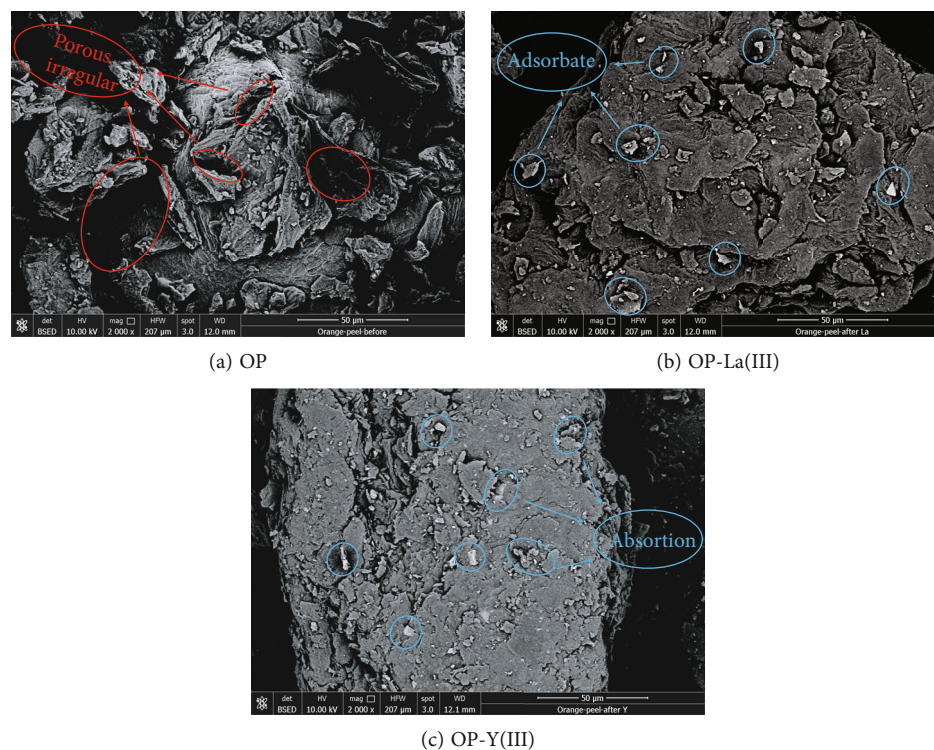
(a) OP

(b) OP-La(III)

(c) OP-Y(III)

Figure 2: SEM images of OP before (a) and after La(III) (b) and Y(III) (c) adsorption.

3. Results and Discussion

3.1. Morphology and Functional Groups of OP

3.1.1. SEM Analysis. Figure 2 displays difference of OP surface structure. Before adsorption, OP embodied a loose and uneven porous structure, which provides plenty of effective sites for the adsorption of La(III) and Y(III). According to the principle of backscattered electron imaging, the microregions with high average atomic numbers in the sample are brighter on the image. Hence, it can be explained that luminous points of images (Figures 2(b) and 2(c)) are the adsorptive distributions of La(III) and Y(III) on the OP surface. The phenomenon reveals that the pore structure of OP is conducive to physical adsorption, and the charge aggregation of particle surface can be illustrated by the outersphere mutual acting (electrostatic) and the surface nucleation of REEs microcrystals in the adsorption process [9, 28].

3.1.2. FTIR Analysis. As shown in Figure 3, the participation of diverse functional groups is proved by FTIR spectra of OP before and after adsorption. The peaks appear at $3428.30 \, \text{cm}^{-1}$, identifying as O-H vibrations that originate from the hydroxyl groups of alcohols, phenols, and carboxylic acids on the adsorbent surface [29]. The peak at $3099.87 \, \text{cm}^{-1}$ attributed to C-H stretching of the alkane groups [30], and the bimodality peaks near $2731.11 \, \text{cm}^{-1}$ represent the stretching of symmetric and asymmetric -CH bond from the aldehyde group [31]. The triple bond and cumulative double bond stretching including the deformation of carbon occurs in several peaks between $2393.93 \, \text{cm}^{-1}$ and $2068.50 \, \text{cm}^{-1}$. The prominent peak at $1757.36 \, \text{cm}^{-1}$ reflects C=O stretching of the nonionized carboxyl groups, which can be associated to organic compounds in OP that contain the dimer form of carboxylic acids, carboxylic esters, ketones, or amides [19]. The peaks at $823.94 \, \text{cm}^{-1}$ and $708.71 \, \text{cm}^{-1}$ are assigned to -CH out-of-plane bending vibration on the aromatic rings [32]. Overall, these functional groups are derived from main components such as pectin, hemicellulose, and lignin [18].

The negligible differences of the OP spectral band before and after adsorption imply that the functional groups remain intact [33]. This is indicative of involvement of ion exchange or surface complexation process. Small range shifts of the peak position indicate that the hydroxyl, carboxyl, and carbonyl groups on the surface of OP played a critical role [30]. It is further supported by the reduction of vibrational intensity [33]. These notions are consistent with the previous finding about the adsorption of metals onto OP [30].

3.2. Batch Adsorption

3.2.1. Effect of Initial pH. The solution pH has been identified as the significant control factor that impacts the adsorption process [34]. As can be seen in Figure 4, the adsorption rate first increases and then decreases with the pH rising from 2.0 to 7.0. The maximum adsorption rates achieved at pH of 6 were 96.99% and 96.84% for La(III) and Y(III), respectively. Further experiments were carried out at pH 6, which is in agreement with the optimum removal of Cd(II) ion by OP at pH 6 as well [30].

The adsorption of La(III) and Y(III) onto OP is intimately dependent on the initial pH that affects the both
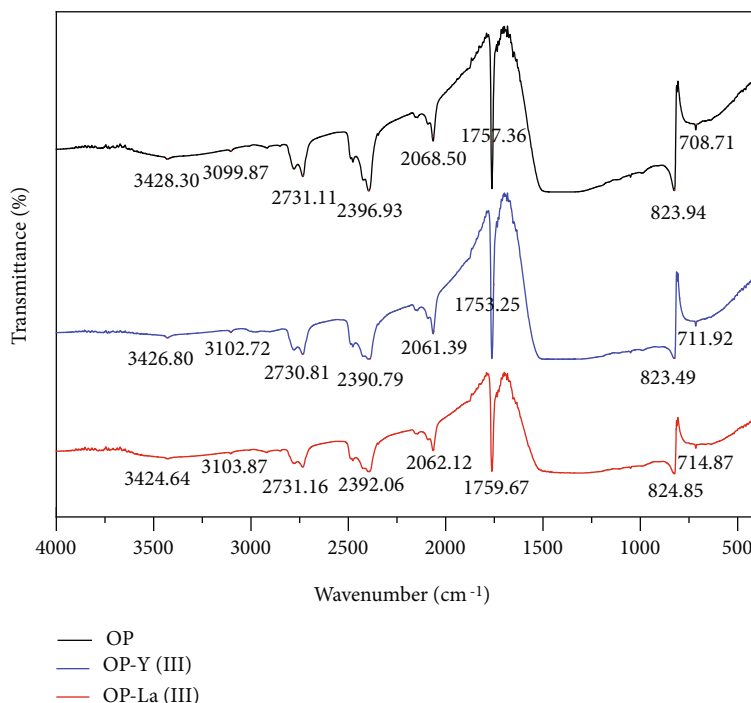
Figure 3: FTIR spectra of OP before and after adsorption for La(III) and Y(III).
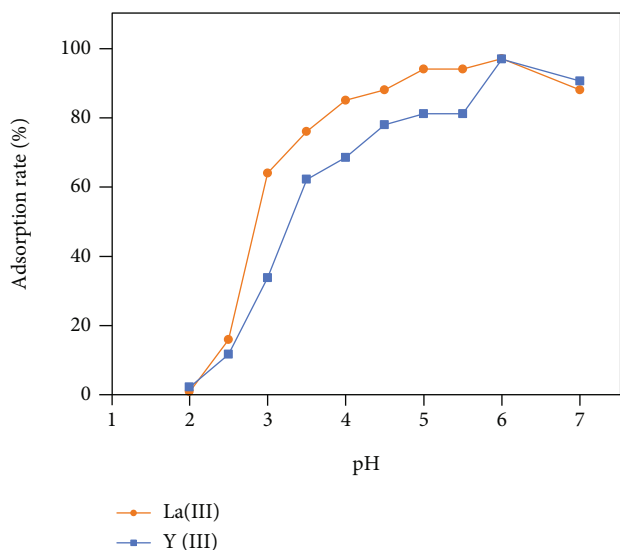

Figure 4: Effect of initial pH on the adsorption of La(III) and Y(III) by OP (room temperature, $C_0 = 32$ mg/L, $S/L = 0.15$ g/100 mL, $t = 2$ h).

metal ion existing speciation and adsorbent surface charge [30]. Additionally, H^+ itself has strong competitive ability for adsorption sites [35]. Lower pH is considered to be a highly acidic medium that allows more protons to protonate active groups. Concurrently, the positive charge regions on OP and the rivalry for adsorption sites between excess H^+ and two rare earth ions lead to lower adsorption rates [30]. With elevated pH, the binding sites perform deprotonation, yielding more negatively charged ligands, followed by an enhancement of adsorption capacity for La(III) and Y(III). From another perspective, other dissociation equilibria and

anion concentration such as hydroxyl ions are increased at alkaline pH (6.0 and above the pKa). Consequently, the elements lanthanum and yttrium probably present in the form of hydroxyl complexes, changing their species into $[M(OH)]_n^{x-}$ [33]. In that case, the adsorption for La(III) and Y(III) onto OP will be degraded. Combining with the FTIR observation of OP, ion exchange and electrostatic interactions exist in the adsorption process, and the potential functional groups such as the O-H, C=O, and C-O groups assume the main responsibility for binding La(III) and Y(III) ions [30].

3.2.2. Effect of Adsorbent Dosage. Figure 5 shows that the adsorption rate of La(III) and Y(III) increases as the dosage equally increases. This trend is attributed to increasing adsorbent particles at fixed concentrations, sufficient amounts of active sites, and available cites around rare earth cations together with larger specific surface area, resulting in stronger cation-adsorbent interactions [17]. The sharp decrease of the Δy value (Δy is the slope divided by the adsorption rates of adjacent dosages) denotes that La(III) and Y(III) are chiefly adsorbed through monolayer swift contact to the filling and absorption. Given that the aggregation of adsorption sites, the total effective site area on the adsorbent surface decreases. Subsequently, due to the free sites are completely occupied, the ions further seek the adsorption sites inside the particles, which involves the induction of functional groups. The phase indicates that the physisorption of the diffusion step is a dominant role [36].

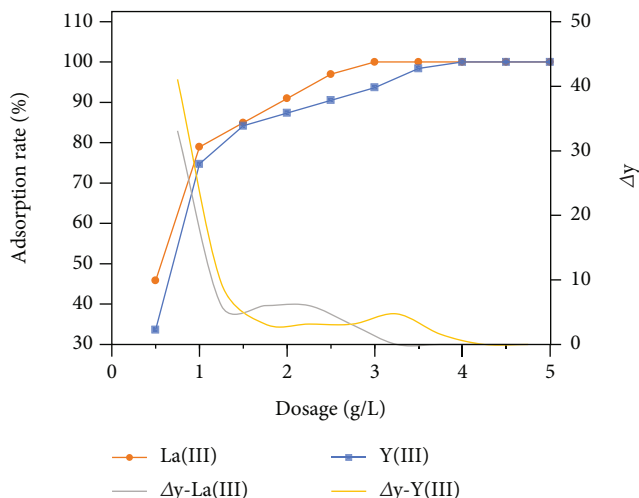*3.2.3. Effect of Temperature.* As indicated from the Figure 6, the adsorption process undergoing two stages as the

FIGURE 5: Effect of dosage on the adsorption of La(III) and Y(III) by OP (room temperature, $C_0 = 32$ mg/L, $V = 100$ mL, pH = 6, $t = 2$ h).
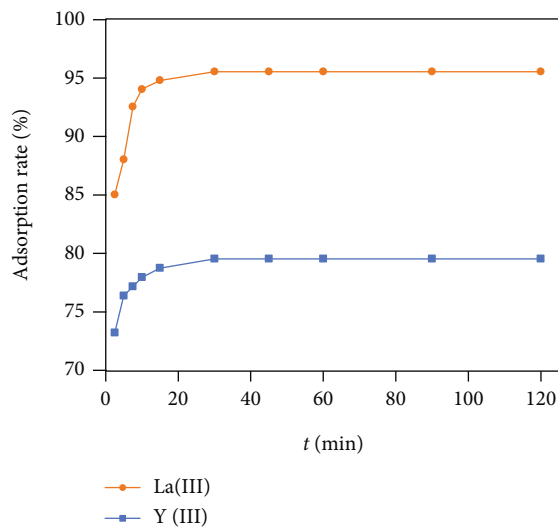

FIGURE 7: Effect of time on the adsorption of La(III) and Y(III) by OP (room temperature, $C_0 = 32$ mg/L, $S/L = 0.15$ g/100 mL, pH = 6).
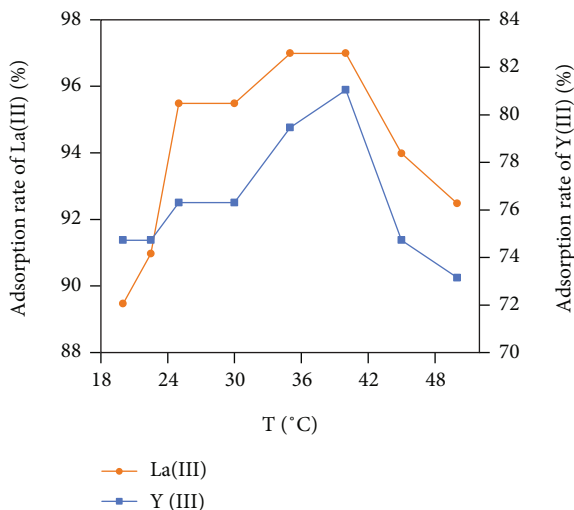
This trend means that the available sites are basically occupied, La(III) and Y(III) progressive enter the micropores of OP, causing a step-down in adsorption velocity owing to the mass transfer resistance on the OP inner wall. This is because the adsorption rate depends on the presence of empty adsorption sites and a high gradient concentration of solute [33]. Prior to the dynamic equilibrium, the OP surface endows with abundant exchangeable sites and porous domains of the adsorbent, which have greater accessibility for the ion binding. As the reaction proceeding, adsorption rates reach the maximum and then remain stable, which indicates that the OP adsorption tends to be saturated.

3.2.5. Effect of Initial Concentration. Further analyses include a set of optimum dosage experiments (La(III) = 2 g/L and Y(III) = 3 g/L) to verify the influence of the initial concentration for OP adsorption performance. Results presented in Figure 8, the adsorption efficiency of La(III) and Y(III) declines near linearly from 100% to 44.64% and 36.81% by increasing the initial concentration. The rapid saturation of active sites cannot meet the growing demand of increasing ion adsorption, thereby limiting the interaction between ions and adsorbent. However, Figure 8(b) reveals that the increment of rare earth ions augmented the driving force for transporting themselves to fully use contact point of adsorbed particles.

By contrast, the adsorption rate of the optimum dosage groups (La(III) = 2 g/L and Y(III) = 3 g/L) is higher than 1.5 g/L groups and shows a more gradual downward trend. This phenomenon is explained by the fact that larger specific surface area contains more exchangeable sites with greater metal binding availability [33]. Therefore, appropriate dosages and concentration allow full access to rare earth cations and adsorbents to enhance their interaction.

FIGURE 6: Effect of temperature on the adsorption of La(III) and Y(III) by OP ($C_0 = 32$ mg/L, $S/L = 0.15$ g/100 mL, pH = 6).

temperature continues to go up. The first one is growth of the adsorption rate, reaching a maximum about 40°C with 95.49% and 76.31% for La(III) and Y(III) by OP, respectively. The higher adsorption rate results from the rising temperature generates driving force to boost the flowability of granules and molecules, thereby facilitating contact between ions and active site of OP [37]. Then, the rates drop sharply in the second stage demonstrates that the process is endothermic and spontaneous [38]. Explicably, overtemperature has the potential to destroy the properties of OP and destabilize rare earth cations, which subdue the positive reaction of adsorption.

3.2.4. Effect of Contact Time. Figure 7 shows that the adsorption was preliminarily faster within 15 min, the remaining adsorption sites are unemployed as a result of inadequate contact time. Whereafter, the adsorption rate becomes sluggish and achieves adsorption equilibrium at about 30 min.

3.3. Adsorption Isotherm. The equilibrium behavior of sorbents can be elucidated by isothermal adsorption models [30]. Langmuir, Freundlich, and Dubinin–Radushkevich

(a)

■ La(III) = 2.0g/L   ■ Y (III) = 3.0g/L
━◆━ La(III) = 1.5g/L   ━■━ Y(III) = 1.5g/L
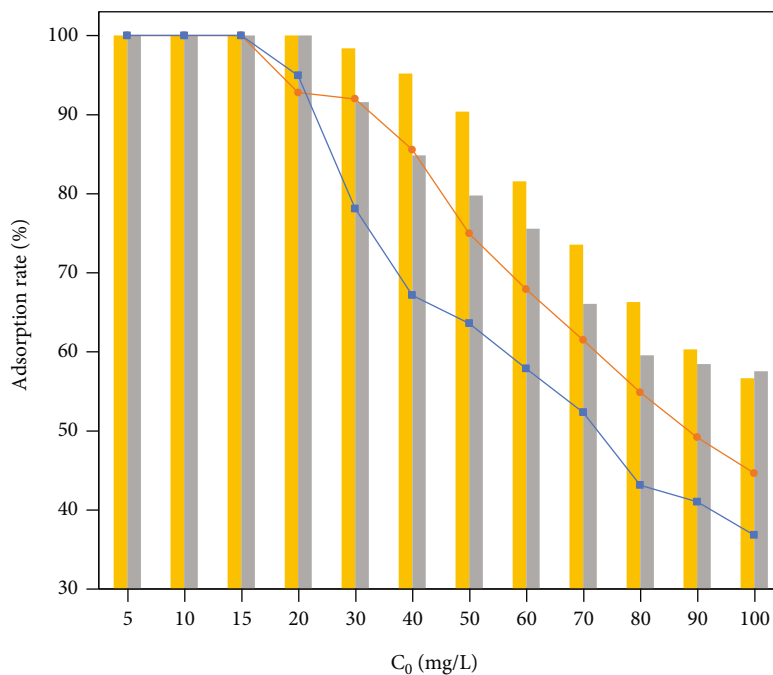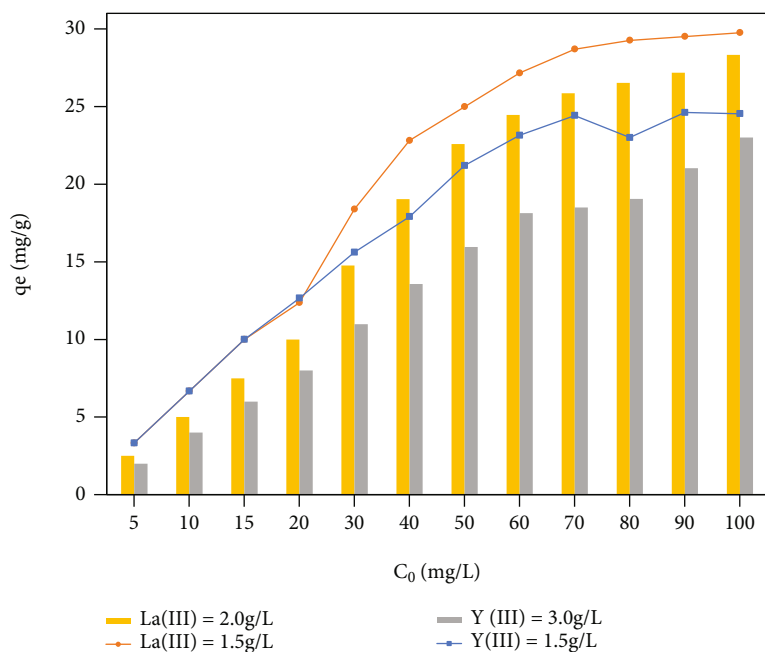
(b)

FIGURE 8: Effect of initial concentration on the adsorption of La(III) and Y(III) onto OP (room temperature, $t = 2$ h, $V = 100$ mL, pH = 6).

(D-R) models are utilized to fit the experimental data (Figure 9). These models describe the adsorption property of adsorbents. One is that the surface may exist as a homogeneous or heterogeneous system; the other is monolayer (single surface contact) or multilayer form (readsorption caused by the adsorption force field). In addition, information concerning the energy distribution of active sites and interactions between adsorbed molecules at the solid-liquid interface is obtained [18, 39].

Generally, the Langmuir isotherm assumes monolayer coverage of the adsorbent surface [40]:

$$\frac{C_e}{q_e} = \frac{C_e}{q_{max}} + \frac{1}{q_{max}K_L}, \qquad (3)$$

where q_{max} (mg/g) represents the maximum monolayer adsorption capacity and K_L (L/mg) is the Langmuir constant
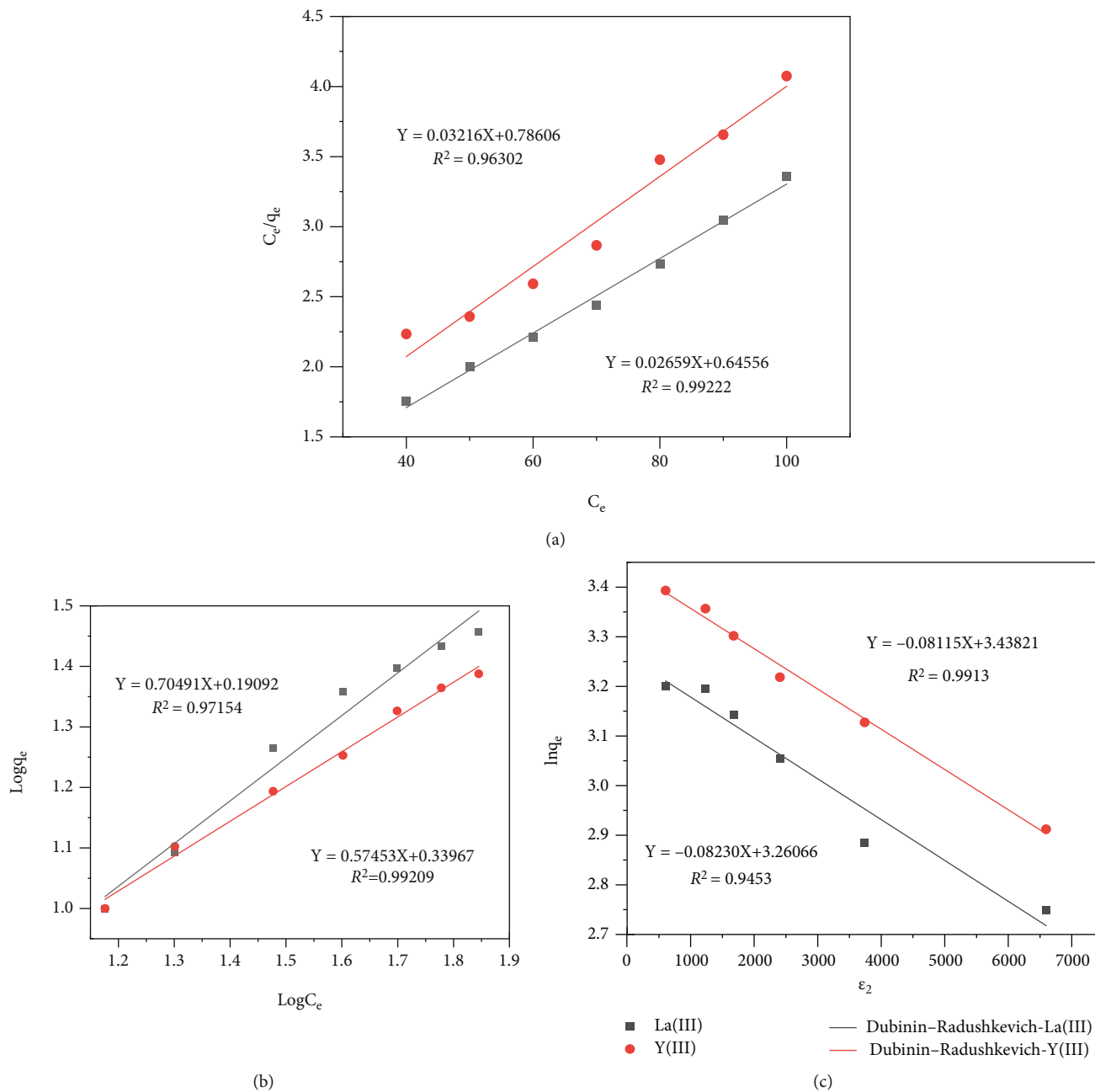
FIGURE 9: (a) Langmuir, (b) Freundlich, and (c) D-R isotherm plots for adsorption of La(III) and Y(III) onto OP.

related to adsorption energy. A linear plot of C_e/q_e versus C_e is obtained for the adsorbent in Figure 9(a). The monolayer adsorption properties can be confirmed by the dimensionless separation factor (R_L):

$$R_L = \frac{1}{1 + K_L C_0}, \tag{4}$$

where C_0 (mg/L) is the initial ion concentration in the solution and the values of R_L lies between 0 and 1, which implies that it is a favorable adsorption, unfavorable when $R_L > 1$ and irreversible when $R_L = 0$ [29].

The Freundlich isotherm assumes multilayer adsorption and a heterogeneous adsorbent surface [35]:

$$\log q_e = \log K_F + \frac{1}{n} \log C_e, \tag{5}$$

where K_F ((mg/g)·(L/mg)$^{1/n}$) is the Freundlich constants and n is the heterogeneity factor that relates to the adsorption capacity and intensity; they can be evaluated from the slope and intercept of the linear plot of $\log q_e$ versus $\log C_e$ in Figure 9(b).

The D-R model describes the adsorption mechanism that does not assume a homogenous surface or constant

adsorption potential [41], which conduce to the explanation regarding homogeneous and heterogeneous adsorption surfaces. The linear plot representation of the D-R equation is defined as

$$\ln q_{\mathrm{e}} = \ln q_{\mathrm{m}} - \beta \varepsilon^2, \tag{6}$$

where q_{m} (mg/g) signifies the saturation adsorption capacity and ε stands for Polanyi potential and is equal to

$$\varepsilon = RT \ln \left(1 + \frac{1}{C_{\mathrm{e}}} \right), \tag{7}$$

The universal gas constant is given as R (8.314 J/(mol·K)) and T is temperature (K). while β (mol²/kJ²) stands for the adsorption free energy. The mean free energy of adsorption, E (kJ/mol), can be calculated from β:

$$E = \frac{1}{\sqrt{-2\beta}}, \tag{8}$$

where E (kJ/mol) can provide prediction about the mechanism of adsorption [30]; when the E value lies between 8 and 16 kJ/mol, it is a chemical ion-exchange process, but when E is less than 8 kJ/mol suggests a physical adsorption process [30, 35].

In this study, the best fitting results among the isothermal models are determined by applying the SSE and EABS error functions [30]:

$$\text{The Sum of Errors Squares (SSE)} = \sum_{i=1}^{n} \left(q_{e-\exp} - q_{e-\mathrm{cal}} \right)^2, \tag{9}$$

$$\text{The Sum of the Absolute Errors (EABS)} = \sum_{i=1}^{n} \left| q_{e-\exp} - q_{e-\mathrm{cal}} \right|. \tag{10}$$

Relevant parameters on the experimental data of the La(III) and Y(III) adsorption are as given in Table 1, and Figure 9 shows the linear plots of isotherm models. The R^2 values taken by the three isothermal models for the two ions are great, which verifies that the three models can describe experimental data with good validity. Whereas, by comparing the SSE and EABS values of the three models, the Langmuir model has the smallest error, which suggests that it gives the most suitable description for the adsorption system on OP. Similar findings have also been mentioned by other literatures, the adsorption isothermal of OP in other metal ion solutions are more relevant to Langmuir model [30, 42], and removal of La(III) and Y(III) by some general adsorbents are also conformed with the Langmuir model [33, 38, 43].

According to the Langmuir mathematical equation, the maximum adsorption capacity of La(III) and Y(III) is estimated to be 37.6 and 31.1 mg/g, respectively. The adsorption mode of La(III) and Y(III) onto the OP surface is predominantly monolayer which provides a single site to attach each ion. Since the $R_{\mathrm{L}} < 1$ for La(III) and Y(III), which indicates that the process has favorable adsorption conditions [30]. It can also be understood that OP has higher adsorption performance than Y(III) in the process of removing La(III) from the aqueous solution.

Although the Freundlich equation is an empirical one, the adequate description of adsorption data in a restricted concentration range is worthy of reference [40]. With the magnitude of $1/n$ between 0.1 and 1.0, which implies that the adsorption process is feasible to separate ions from the aqueous solution with greater heterogeneous adsorption site and energy distribution ($n > 1$). D-R parameter, E of La(III) and Y(III), is found to be 7.85 and 7.80 kJ/mol, since the value of E is smaller than 8 kJ/mol; the adsorption mechanism is physical reaction in nature [30, 35].

3.4. Adsorption Kinetics Studies. The pseudofirst-order (Equation (11)) and pseudosecond-order (Equation (12)) are performed to investigate adsorption kinetics of La(III) and Y(III) onto OP.

$$\log (q_{\mathrm{e}} - q_t) = \log q_{\mathrm{e}} - \frac{k_1 t}{2.303}, \tag{11}$$

$$\frac{t}{q_t} = \frac{1}{k_2 q_{\mathrm{e}}^2} + \frac{t}{q_{\mathrm{e}}}, \tag{12}$$

$$H = k_2 q_{\mathrm{e}}^2, \tag{13}$$

where q_t (mg/g) is the adsorption amount at time t and k_1 (1/min) and k_2 (g/(mg·min)) are the rate constants for the pseudofirst-order and pseudosecond-order, respectively; k_2 is further used to measure the adsorption capacity and initial adsorption rate constant H (mg/(g·min)) (Equation (13)) [31].

The fitting parameters and the linear plot are depicted in Table 2 and Figure 10. It is observed from the results that biosorption kinetics of La(III) and Y(III) on OP are well contoured by the pseudosecond-order equation. Consequently, the adsorption process mainly acts as the rate-controlling factor. On the other hand, the q_{e} values suggest that La(III) are adsorbed more sufficiently than Y(III). According to the previous conclusions, this is due to the weaker repulsion between La(III) and sorbents, facilitating the activities of the remaining adsorptive sites. The H values show that the adsorption of Y(III) onto OP reach equilibrium slightly faster owing to the greater external diffusion rate of Y(III) couple with a small diameter [30].

3.5. Comparison of Various Adsorbents. Other untreated adsorbents for La(III) and Y(III) are presented in Table 3. The results exhibit better adsorption capacity of OP adsorbent compared to the leaf, shell, and bone waste. As expected, modification of materials has increased their adsorption efficiencies, whereas the assessment of adsorbent more to the point if efficiency, availability, reusability, and economic aspect are considered [30]. It is noteworthy that the unmodified wastes also have competitive sorption capacity.

TABLE 1: Isotherm parameters for La(III) and Y(III) adsorption onto OP.

Model	Parameter	La(III)	Y(III)
q_m(exp)		31.2634	27.6044
Langmuir	q_{max}	37.6081	31.0945
	K_L	0.0412	0.0409
	R_L (5-100 mg/L)	0.8292-0.1954	0.8302-0.1964
	R^2	0.9922	0.9630
	SSE	75.7625	22.7167
	EABS	21.8587	14.5486
Freundlich	K_F	1.2104	1.4045
	n	1.4186	1.7406
	R^2	0.9715	0.9921
	SSE	172.3507	398.9251
	EABS	37.3225	62.5976
Dubinin-Radushkevich (D-R)	K_{D-R}	0.00812	0.00823
	q_m	31.1311	26.0667
	E	7.8493	7.7945
	R^2	0.9913	0.9453
	SSE	97.3420	125.9459
	EABS	20.8711	26.0753

TABLE 2: Parameters of kinetic models for adsorption of La(III) and Y(III) onto OP.

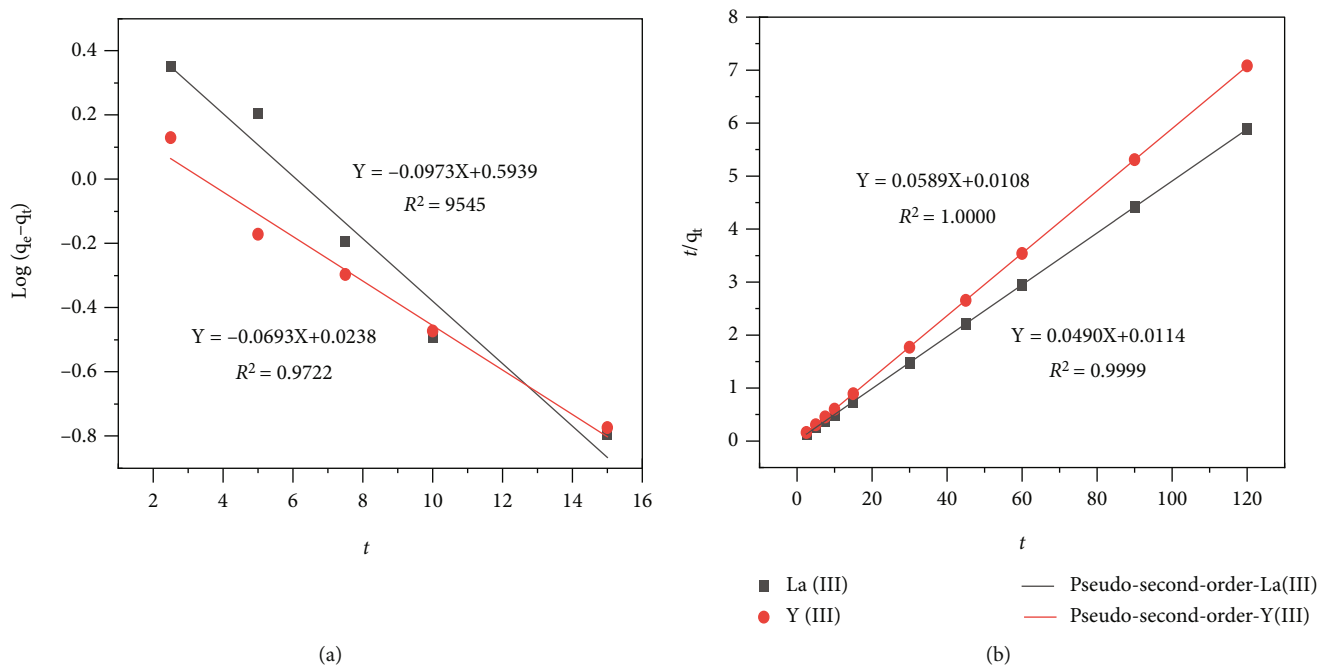| Type	q_e(exp)	Pseudofirst-order			Pseudosecond-order			
		K_1	q_e	R^2	K_2	q_e	H	R^2
La(III)	20.3705	0.2241	3.9251	0.9545	0.2100	20.4270	87.612	0.9999
Y (III)	16.9524	0.1596	1.0562	0.9722	0.3213	16.9887	92.728	1.0000

FIGURE 10: (a) Pseudofirst-order and (b) pseudosecond-order kinetic linear plots for adsorption of La(III) and Y(III) onto OP.

TABLE 3: Comparison of orange peel adsorption capacity with other natural adsorbents for removal of La(III) and Y(III).

Adsorbents	Metals	Particle size (μm)	Concentration (mg/L)	Dose (g/L)	q_{m} (mg/g)	References
Orange peel	La(III)	125-150	32	2	37.61	Present study
	Y(III)	125-150	32	3	31.10	
Durian rind	La(III)	<500	60-160	2.5	71	[33]
	Y(III)	<500	60-160	2.5	35	
Durian rind pectin	La(III)	<500	160	2.5	41.2	[46]
Pinus brutia leaf	La(III)	125	25-300	4	22.94	[38]
Platanus orientalis leaf	La(III)	125	25-300	4	28.65	[47]
Pleurotus ostreatus	Y(III)	125-250	50-350	10	45.45	[48]
Pleurotus ostreatus	La(III)	125-250	50-350	10	54.54	[49]
Orange peel	La(III)	425-600	250	2.5	125	[50]
Banana (peel, stem)	Y(III)	250-800	100-300	1	<35,50	[39]
Banana peel	La(III)	65	20-200	1	47.8	[51]
Grapefruit peel	La(III)	<355	20	2.5	171.20	[52]
Bone powder	La(III)	—	5-500	20	8.7	[40]
Pectin-chitosan composites	La(III)	—	10-180	1	22	[43]
	Y(III)	—	10-180	1	23	
Buccinum tenuissimum shell	Lanthanides	>600	0.01-0.5	2	6.2	[53]

Among biosorbents, OP has attracted more attention. The q_{m} of the batch adsorption of Cd(II) by natural OP powder is 128.23 mg/g [30], the maximum adsorption capacity of cellulosic OP for Cu(II) is 63 mg/g [44], and the removal rate of Cr(VI) from wastewater with natural OP sorbent is higher than 95% [45]. It is agreed that this material has promising applications for effluent treatment.

4. Conclusions

The study herein indicates that OP as an economical adsorbent in practice is a good alternative for costly adsorbents. The adsorption rates are as high as 93.98% and 90.52% at a pH of 6.0, temperature of 40°C, and dosage of La(III) and Y(III) are 2 g/L and 3 g/L in initial ion concentration of 32 mg/L with the contact time more than 30 min.

The priority of adsorption equilibrium data fitting obeys this order: Langmuir > Dubinin-Radushkevich > Freundlich. The adsorption process is dominated by monolayer chemisorption. In addition, the adsorption kinetics of La(III) and Y(III) onto OP are preferable described by the pseudosecond-order model. The characterization results reveal that the metal ion adsorption onto OP is a spontaneous physical-chemical interaction, and the OP surface sites, porous domains, and functional groups are contributed to the adsorption mechanism. In accordance with the present study finding, natural OP presents a promising biosorbent for eliminating La(III) and Y(III) from the aqueous solution.

Data Availability

The data that support the findings of this study are available from the corresponding author (VS) upon reasonable request.

Conflicts of Interest

The authors declared that there is no conflict of interest.

Acknowledgments

References

[1] Y. F. Xiao, Y. Y. Chen, Z. Y. Feng et al., "Leaching characteristics of ion-adsorption type rare earths ore with magnesium sulfate," *Transactions of Nonferrous Metals Society of China*, vol. 25, no. 11, pp. 3784–3790, 2015.

[2] Z. Q. Guo, K. Zhao, J. F. Jin, W. Yuan, and C. Liang, "Problems facing ion adsorption type rare earth exploitation and research progresses on green extraction," *Chemical Industry and Engineering Progress*, vol. 38, no. 7, pp. 3425–3433, 2019.

[3] H. F. Zhan, H. S. Wang, Y. Pan, H. H. Sun, and Z. W. Liu, "Measurement and analysis of ion-type rare earth mine wastewater," *Journal of the Chinese Society of Rare Earths*, vol. 38, no. 4, pp. 550–556, 2020.

[4] K. Binnemans, P. T. Jones, T. Müller, and L. Yurramendi, "Rare earths and the balance problem: how to deal with changing markets?," *Journal of Sustainable Metallurgy*, vol. 4, pp. 126–146, 2018.

[5] G. C. Han, J. Y. Ning, Z. Yu et al., "Hazard assessment of the effects of rare earth element lanthanum on health," *Journal of Toxicology*, vol. 33, no. 6, 443 pages, 2019.

[6] D. Das, S. Jaya, and N. Das, "Recovery of lanthanum (III) from aqueous solution using biosorbents of plant and animal origin: batch and column studies," *Minerals Engineering*, vol. 69, pp. 40–56, 2014.

[7] I. Anastopoulos, A. Bhatnagar, and E. C. Lima, "Adsorption of rare earth metals: a review of recent literature," *Journal of Molecular Liquids*, vol. 221, pp. 954–962, 2016.

[8] X. Gao, L. Jiang, Y. Mao, B. Yao, and P. Jiang, "Progress, challenges, and perspectives of bioleaching for recovering heavy metals from mine tailings," *Adsorption Science and Technology*, vol. 2021, article 9941979, 13 pages, 2021.

[9] V. S. Munagapati, J. C. Wen, C. L. Pan, Y. Gutha, and J. H. Wen, "Enhanced adsorption performance of reactive red 120 azo dye from aqueous solution using quaternary amine modified orange peel powder," *Journal of Molecular Liquids*, vol. 285, no. 4, pp. 375–385, 2019.

[10] A. el Nemr, R. M. Aboughaly, A. el Sikaily, S. Ragab, M. S. Masoud, and M. S. Ramadan, "Microporous nano-activated carbon type I derived from orange peel and its application for Cr(VI) removal from aquatic environment," *Biomass Conversion and Biorefinery*, vol. 1, pp. 1–19, 2020.

[11] I. C. Afolabi, S. I. Popoola, and O. S. Bello, "Modeling pseudo-second-order kinetics of orange peel-paracetamol adsorption process using artificial neural network," *Chemometrics and Intelligent Laboratory Systems*, vol. 203, p. 104053, 2020.

[12] B. P. Mora, F. A. Bertoni, M. F. Mangiameli, J. C. González, and S. E. Bellú, "Batch and fixed-bed column studies of selenite removal from contaminated water by orange peel-based sorbent," *Water Science and Engineering*, vol. 13, no. 4, pp. 307–316, 2020.

[13] V. S. Munagapati and D. S. Kim, "Adsorption of anionic azo dye Congo Red from aqueous solution by Cationic Modified Orange Peel Powder," *Journal of Molecular Liquids*, vol. 220, pp. 540–548, 2016.

[14] M. Salman, M. Athar, and U. Farooq, "Biosorption of heavy metals from aqueous solutions using indigenous and modified lignocellulosic materials," *Reviews in Environmental Science and Biotechnology*, vol. 14, pp. 211–228, 2015.

[15] N. Das and D. Das, "Recovery of rare earth metals through biosorption: an overview," *Journal of Rare Earths*, vol. 31, no. 10, pp. 933–943, 2013.

[16] R. M. Naik, "Relationship between the Freundlich adsorption constants K and 1/N hydrophobic adsorption," *Indian Journal of Chemical Technology*, vol. 25, pp. 300–305, 2018.

[17] A. Pandiarajan, R. Kamaraj, S. Vasudevan, and S. Vasudevan, "OPAC (orange peel activated carbon) derived from waste orange peel for the adsorption of chlorophenoxyacetic acid herbicides from water: adsorption isotherm, kinetic modelling and thermodynamic studies," *Bioresource Technology*, vol. 261, pp. 329–341, 2018.

[18] C. Tejada-Tovar, A. Herrera-Barros, A. Villabona-Ortíz, Á. González-Delgado, and J. Núñez-Zarur, "Hexavalent chromium adsorption from aqueous solution using orange peel modified with calcium chloride: equilibrium and kinetics study," *Indian Journal of Science and Technology*, vol. 11, no. 17, pp. 1–10, 2018.

[19] C. Zhang, X. Zhou, and F. Gao, "Preparation of orange peel loaded Zn/Al-HT and its adsorption for Cr(VI) in water," *IOP Conference Series: Earth and Environmental Science*, vol. 687, no. 1, p. 012073, 2021.

[20] M. T. Amin, A. A. Alazba, and M. Shafiq, "Application of the biochar derived from orange peel for effective biosorption of copper and cadmium in batch studies: isotherm models and kinetic studies," *Arabian Journal of Geosciences*, vol. 12, no. 2, pp. 46–58, 2019.

[21] C. Tejada-Tovar, Á. González-Delgado, and A. Villabona-Ortíz, "Adsorption kinetics of orange peel biosorbents for Cr(VI) uptake from water," *Contemporary Engineering Sciences*, vol. 11, no. 24, pp. 1185–1193, 2018.

[22] S. Pavithra, G. Thandapani, S. S et al., "Batch adsorption studies on surface tailored chitosan/orange peel hydrogel composite for the removal of Cr(VI) and Cu(II) ions from synthetic wastewater," *Chemosphere*, vol. 271, no. 12, p. 129415, 2021.

[23] L. X. Wang, X. T. Zhou, and Z. Q. Luo, "Research Progress of the properties and mechanism of heavy metal Pb^{2+} absorbed by agricultural and forestry waste in wastewater," *Materials Reports*, vol. 34, no. 17, pp. 119–127, 2020.

[24] N. C. Feng and X. Y. Guo, "Characterization of adsorptive capacity and mechanisms on adsorption of copper, lead and zinc by modified orange peel," *Transactions of Nonferrous Metals Society of China*, vol. 22, pp. 1224–1231, 2012.

[25] N. C. Feng, X. Y. Guo, and S. Liang, "Adsorption study of copper(II) by chemically modified orange peel," *Journal of Hazardous Materials*, vol. 164, no. 2-3, pp. 1286–1292, 2009.

[26] X. F. Zhang, J. X. Xiang, J. Q. Tian, and Y. Xie, "Preparation of activated carbons from waste cCitrus dregs by. Na_2CO_3、K_2CO_3 and KOH and performance analysis," *Chemical Reagents*, vol. 43, no. 3, pp. 274–279, 2021.

[27] Z. G. Xie, F. Y. Ji, X. M. Qiu, and H. Huang, "Preparation and characterization of mesoporous activated carbon from orange peel," *Journal of Functional Materials*, vol. 40, no. 4, pp. 645–649, 2009.

[28] Z. S. Birungi and E. Chirwa, "The kinetics of uptake and recovery of lanthanum using freshwater algae as biosorbents: comparative analysis," *Bioresource Technology*, vol. 160, no. 5, pp. 43–51, 2014.

[29] A. A. Ayalew and T. A. Aragaw, "Utilization of treated coffee husk as low-cost bio-sorbent for adsorption of methylene blue," *Adsorption Science and Technology*, vol. 38, no. 5-6, pp. 205–222, 2020.

[30] T. F. Akinhanmi, E. A. Ofudje, A. I. Adeogun, P. Aina, and I. M. Joseph, "Orange peel as low-cost adsorbent in the elimination of Cd(II) ion: kinetics, isotherm, thermodynamic and optimization evaluations," *Bioresources and Bioprocessing*, vol. 7, no. 1, pp. 1–16, 2020.

[31] C. Pathirana, A. M. Ziyath, K. B. S. N. Jinadasa, P. Egodawatta, and A. Goonetilleke, "Mathematical modelling of the influence of physico-chemical properties on heavy metal adsorption by biosorbents," *Chemosphere*, vol. 255, p. 126965, 2020.

[32] I. A. Altameemi and M. A. Thuraya, "Removal of manganese (Mn^{2+}) from aqueous solution by low-cost adsorbents and study the adsorption thermodynamics and kinetics," *Journal of Physics: Conference Series*, vol. 1773, no. 1, p. 012038, 2021.

[33] E. Kusrini, A. Usman, F. A. Sani, L. D. Wilson, and M. A. A. Abdullah, "Simultaneous adsorption of lanthanum and yttrium from aqueous solution by durian rind biosorbent," *Environmental Monitoring and Assessment*, vol. 191, no. 8, pp. 1–8, 2019.

[34] B. Thomas, E. P. Shilpa, and L. K. Alexander, "Role of functional groups and morphology on the pH-dependent adsorption of a cationic dye using banana peel, orange peel, and neem leaf bio-adsorbents," *Emergent Materials*, vol. 35, pp. 1–9, 2021.

[35] A. A. Alghamdi, A. B. al-Odayni, N. Abduh, S. A. Alramadhan, M. T. Aljboar, and W. S. Saeed, "Adsorptive performance of polypyrrole-based KOH-activated carbon for the cationic dye

crystal violet: kinetic and equilibrium studies," *Adsorption Science and Technology*, vol. 2021, article 5527594, 11 pages, 2021.

[36] C. Pathirana, A. M. Ziyath, K. B. S. N. Jinadasa, P. Egodawatta, S. Sarina, and A. Goonetilleke, "Quantifying the influence of surface physico-chemical properties of biosorbents on heavy metal adsorption," *Chemosphere*, vol. 234, pp. 488–495, 2019.

[37] M. B. Amar, K. Walha, and V. Salvadó, "Valorisation of pine cone as an efficient biosorbent for the removal of Pb(II), Cd(II), Cu(II), and Cr(VI)," *Adsorption Science and Technology*, vol. 12, p. 12, 2021.

[38] C. Kütahyali, S. Sert, B. Çetinkaya, S. Inan, and M. Eral, "Factors affecting lanthanum and cerium biosorption onPinus brutiaLeaf powder," *Separation Science and Technology*, vol. 45, no. 10, pp. 1456–1462, 2010.

[39] B. Lapo, J. J. Bou, J. Hoyo et al., "A potential lignocellulosic biomass based on banana waste for critical rare earths recovery from aqueous solutions," *Environmental Pollution*, vol. 264, p. 114409, 2020.

[40] M. Butnariu, P. Negrea, L. Lupa et al., "Remediation of rare earth element pollutants by sorption process using organic natural sorbents," *International Journal of Environmental Research and Public Health*, vol. 12, no. 9, pp. 11278–11287, 2015.

[41] A. Daouda, A. T. Honorine, N. G. Bertrand, D. Richard, and R. Domga, "Adsorption of Rhodamine B onto Orange Peel Powder," *American Journal of Chemistry*, vol. 9, no. 5, pp. 142–149, 2019.

[42] L. Salisu and M. B. Ibrahim, "Analysis of some sorption isotherms for the removal of Ni^{2+}, Pb^{2+} and Cu^{2+} using orange peel adsorbent," *Bayero Journal of Pure and Applied Sciences*, vol. 10, no. 1, pp. 414–417, 2017.

[43] D. Kong, E. Kusrini, and L. D. Wilson, "Binary pectin-chitosan composites for the uptake of lanthanum and yttrium species in aqueous media," *Micromachines*, vol. 12, no. 5, p. 478, 2021.

[44] S. Guiza, "Biosorption of heavy metal from aqueous solution using cellulosic waste orange peel," *Ecological Engineering*, vol. 99, pp. 134–140, 2017.

[45] T. J. Jisha, C. H. Lubna, and V. Habeeba, "Removal of Cr (VI) using orange peel as an adsorbent," *IJARIIE*, vol. 3, no. 4, pp. 276–283, 2017.

[46] E. Kusrini, W. Wicaksono, C. Gunawan, N. Z. A. Daud, and A. Usman, "Kinetics, mechanism, and thermodynamics of lanthanum adsorption on pectin extracted from durian rind," *Journal of Environmental Chemical Engineering*, vol. 6, no. 5, pp. 6580–6588, 2018.

[47] Ş. Sert, C. Kütahyali, S. İnan, Z. Talip, B. Çetinkaya, and M. Eral, "Biosorption of lanthanum and cerium from aqueous solutions by _Platanus orientalis_ leaf powder," *Hydrometallurgy*, vol. 90, no. 1, pp. 13–18, 2008.

[48] S. S. Hussien and O. A. Desouky, "Biosorption studies on yttrium using low cost pretreated biomass of Pleurotus ostreatus," *International conference on radiation research and applied science*, vol. 10, pp. 139–150, 2014.

[49] S. S. Hussien, "Biosorption of lanthanum from aqueous solution using Pleurotus ostreatus basidiocarps," *International Journal of Biotechnology*, vol. 2, no. 3, pp. 26–36, 2014.

[50] C. Varshini and N. Das, "Relevant approach to assess the performance of biowaste materials for the recovery of lanthanum (III) from aqueous medium," *Research Journal of Pharmaceutical, Biological and Chemical Sciences*, vol. 5, no. 6, pp. 88–94, 2014.

[51] O. A. Oyewo, M. S. Onyango, and C. Wolkersdorfer, "Lanthanides removal from mine water using banana peels nanosorbent," *International journal of Environmental Science and Technology*, vol. 15, no. 6, pp. 1265–1274, 2017.

[52] M. Torab-Mostaedi, M. Asadollahzadeh, A. Hemmati, and A. Khosravi, "Biosorption of lanthanum and cerium from aqueous solutions by grapefruit peel: equilibrium, kinetic and thermodynamic studies," *Research on Chemical Intermediates*, vol. 41, no. 2, pp. 559–573, 2015.

[53] Y. Koto, N. Kano, Y. Wang, N. Sakamoto, and H. Imaizumi, "Biosorption of lanthanides from aqueous solutions using pretreated Buccinum tenuissimum shell biomass," *Bioinorganic Chemistry and Applications*, vol. 2010, Article ID 804854, 10 pages, 2010.